

Better Verified Explanations with Applications to Incorrectness and Out-of-Distribution Detection

Min Wu, Xiaofu Li, Haoze Wu, Clark Barrett

Department of Computer Science
Stanford University
{minwu, lixiaofu, haozewu, barrett}@cs.stanford.edu

Abstract

Building on VERIX (VERified explainability) (Wu, Wu, and Barrett 2023), a system for producing *optimal verified explanations* for machine learning model outputs, we present VERIX+, which significantly improves both the *size* and the *generation time* of verified explanations. We introduce a bound propagation-based sensitivity technique to improve the size, and a binary search-based traversal with confidence ranking for improving time—the two techniques are orthogonal and can be used independently or together. We also show how to adapt the QuickXplain (Junker 2004) algorithm to our setting to provide a trade-off between size and time. Experimental evaluations on standard benchmarks demonstrate significant improvements on both metrics, e.g., a size reduction of 38% on the GTSRB dataset and a time reduction of 90% on MNIST. We also explore applications of our verified explanations and show that explanation size is a useful proxy for both incorrectness detection and out-of-distribution detection.

1 Introduction

Explainable AI aims to extract a set of reasoning steps from the decision-making processes of otherwise opaque AI systems, thus making them more understandable and trustworthy to humans. Well-known work on explainable AI includes model-agnostic explainers, such as LIME (Ribeiro, Singh, and Guestrin 2016), SHAP (Lundberg and Lee 2017), and Anchors (Ribeiro, Singh, and Guestrin 2018), which provide explanations for neural networks by constructing a local model around a given input or identifying a subset of input features as “anchors” that (ideally) ensure a model’s decision. While such methods can produce explanations efficiently, they do not provide *formal* guarantees and thus may be inadequate in high-stakes scenarios, e.g., when transparency and fairness are paramount.

Formal explainable AI (Marques-Silva and Ignatiev 2022) aims to compute explanations that *verifiably* ensure the invariance of a model’s decision. One such explanation is a minimal set of input features with the property that regardless of how the *remaining* features are perturbed, the prediction remains unchanged. The intuition is that these features capture an amount of (explicit or implicit) information in the input that is sufficient to preserve the current decision. The simplest approaches allow *unbounded* perturbations (Ignatiev, Narodytska, and Marques-Silva 2019; Shih, Choi, and Darwiche 2018; Darwiche and Hirth 2020), which may be overly

lenient in some cases, potentially leading to explanations that are too course-grained to be useful. As an alternative, (La Malfa et al. 2021) and (Wu, Wu, and Barrett 2023) generalize these approaches by allowing both *bounded* and *unbounded* perturbations, computing explanations with respect to such perturbations for natural language processing and perception models, respectively. The former primarily perturbs each word in a text with a finite set of its k closest neighbors and thus has a discrete perturbation space; the latter considers ϵ -ball perturbations over continuous and dense input spaces. The algorithm presented in (Wu, Wu, and Barrett 2023) is a naive and well-known approach: it simply traverses the features one by one and checks formally whether any of them can be discarded. This approach sometimes yields overly conservative explanations that are inefficient to compute.

In this paper, we explore methods for computing better explanations by significantly improving both the *size* and the *generation time*. We also demonstrate two applications that illustrate the usefulness of such explanations in practice. Our contributions can be summarized as follows.

- We utilize *bound propagation*-based techniques to obtain more fine-grained feature-level sensitivity information, leading to better traversal orders which in turn produce smaller explanation sizes.
- We propose a *binary search*-inspired traversal approach to enable processing features in a batch manner, thus significantly reducing the *time* required to generate explanations. We also incorporate a simple but efficient *confidence ranking* strategy to further reduce time.
- We adapt the QuickXplain algorithm (Junker 2004) to provide a *trade-off* between explanation *size* and generation *time*, and notice that our adaptation is an optimization of (Huang and Marques-Silva 2023).
- We demonstrate the usefulness of our explanations with practical applications to detecting *incorrect* predictions and *out-of-distribution* samples.

2 VERIX+: VERified eXplainability plus

Let f be a neural network and \mathbf{x} an input consisting of m -dimensional features $\langle x_1, \dots, x_m \rangle$. The set of feature indices $\{1, \dots, m\}$ is written as $\Theta(\mathbf{x})$, or simply Θ , when the context is clear. To denote a subset of indices, we use $\mathbf{A} \in \Theta(\mathbf{x})$, and $\mathbf{x}_{\mathbf{A}}$ denotes the features that are indexed by the indices in \mathbf{A} .

We write $f(\mathbf{x}) = c$ for both regression models (c is a single quantity) and classification models ($c \in C$ is one of a set of possible labels). For the latter case, we use $\mathbf{y} = \langle y_1, \dots, y_n \rangle$ to denote confidence values for each label in C , e.g., the predicted class $c = \arg \max(\mathbf{y})$. For image classification tasks, \mathbf{x} is an image of m pixels, the values in \mathbf{y} represent the confidence values for each of the n labels in C , and y_c is the maximum value in \mathbf{y} , where c is the predicted label.

2.1 Optimal verified explanations

We adopt the definition of *optimal robust explanations* from (La Malfa et al. 2021; Wu, Wu, and Barrett 2023) (see also (Shih, Choi, and Darwiche 2018; Ignatiev, Narodytska, and Marques-Silva 2019; Darwiche and Hirth 2020)). For a neural network f and an input \mathbf{x} , we compute a minimal subset of \mathbf{x} , denoted by \mathbf{x}_A , such that any ϵ -perturbations imposed on the remaining features do not change the model’s prediction.

Definition 2.1 (Optimal Verified Explanation (Wu, Wu, and Barrett 2023)). Given a neural network f , an input \mathbf{x} , a manipulation magnitude ϵ , and a discrepancy δ , a *verified explanation* with respect to norm $p \in \{1, 2, \infty\}$ is a set of input features \mathbf{x}_A such that if $\mathbf{B} = \Theta(\mathbf{x}) \setminus \mathbf{A}$, then

$$\forall \mathbf{x}'_{\mathbf{B}}. \|\mathbf{x}_{\mathbf{B}} - \mathbf{x}'_{\mathbf{B}}\|_p \leq \epsilon \implies |f(\mathbf{x}) - f(\mathbf{x}')| \leq \delta, \quad (1)$$

where $\mathbf{x}'_{\mathbf{B}}$ is some perturbation on the *irrelevant* features $\mathbf{x}_{\mathbf{B}}$ and \mathbf{x}' is the input variant combining \mathbf{x}_A and $\mathbf{x}'_{\mathbf{B}}$. We say that the verified explanation \mathbf{x}_A is *optimal* if

$$\forall x \in \mathbf{x}_A. \exists x', \mathbf{x}'_{\mathbf{B}}. \|(x \cup \mathbf{x}_{\mathbf{B}}) - (x' \cup \mathbf{x}'_{\mathbf{B}})\|_p \leq \epsilon \wedge |f(x \cup \mathbf{x}_{\mathbf{B}}) - f(x' \cup \mathbf{x}'_{\mathbf{B}})| > \delta, \quad (2)$$

where x' is some perturbation of $x \in \mathbf{x}_A$ and \cup denotes concatenation of features.

Such explanations are both *sound* and *optimal* by Equations (1) and (2), respectively (Wu, Wu, and Barrett 2023). Note that the optimality we define here is *local* as it computes a minimal (not minimum) subset. A minimum subset is called a *global* optimum, also known as the cardinality-minimal explanation (Ignatiev, Narodytska, and Marques-Silva 2019). However, finding the global optimum is generally too computationally expensive to be practically useful, as it requires searching over an exponential number of local optima.

2.2 Workflow of VERIX+ in a nutshell

We present the overall workflow of our VERIX+ framework in Figure 1. Starting from the left, the inputs are a network f and an input \mathbf{x} . The first step is to obtain a sensitivity map of all the input features and, by ranking their individual sensitivity, produce a traversal order. We introduce a new bound propagation-based technique (Algorithm 1) for obtaining more meaningful sensitivity maps and thus better traversal orders, which, in turn, reduce explanation sizes.

The traversal order is then passed to the main traversal algorithm, which computes optimal verified explanations. We propose two new optimizations, one based on binary search (Algorithm 2) and one adapted from the well-known QuickXplain algorithm (Junker 2004) (Algorithm 4). These can significantly reduce computation time compared to the

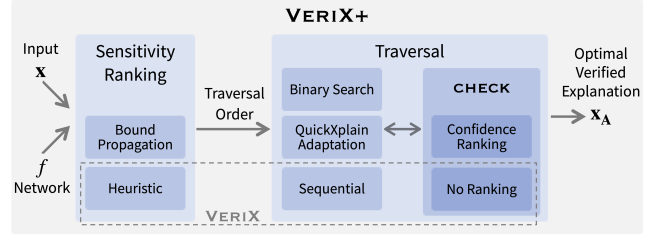


Figure 1: The VERIX+ framework.

existing sequential method, which processes features one by one. The key difference between these two is that the former reduces the time but not the size, as it does not change the traversal order, whereas the latter improves both size and time. Compared to the binary search-based technique, the QuickXplain technique computes comparatively smaller-sized explanations but takes more time, thus providing an alternative point in the size-time trade-off.

The CHECK procedure (Algorithm 3) is used by the traversal methods to formally check the soundness of a candidate explanation. We also add a simple but efficient confidence ranking algorithm which further reduces generation time. The confidence ranking is orthogonal to the other optimizations and benefits all three traversal approaches mentioned above.

Once the optimal verified explanation \mathbf{x}_A has been computed for network f and input \mathbf{x} , it can be used in various ways. We highlight two applications: detecting incorrect predictions and detecting out-of-distribution examples. We show that explanation size is a useful proxy for both tasks. These applications are described in detail in Sections 4.3 and 4.4.

3 Methodological advances for explanation size and generation time

In this section, we discuss in detail several optimizations for improving both the *size* and the *generation time* of optimal verified explanations. The bound propagation-based sensitivity ranking discussed in Section 3.1 improves size, and the binary search-based traversal discussed in Section 3.2 improves time, so does the confidence ranking discussed in Section 3.3. Section 3.4 discusses how an adaptation of the QuickXplain algorithm (Junker 2004) enables an additional size-time trade-off.

3.1 Improving size: a bound propagation-based traversal order

In (Wu, Wu, and Barrett 2023), a traversal order is computed based on a heuristic that measures how sensitive a model’s confidence is to each individual feature x_i by imposing simple feature deletion ($x_i = 0$) or reversal ($1 - x_i$). Although this produces a reasonable ranking of the input indices, it ignores the fact that explanations are based on ϵ -perturbations. We show how utilizing the perturbation information at the sensitivity phase can produce better traversal orders.

Procedure TRAVERSALORDER in Algorithm 1 computes ϵ -bounds for each feature of the input and then ranks these bounds to obtain an order of feature indices. We introduce variables $\hat{\mathbf{x}}$ which represent symbolic inputs to f (Line 3).

Algorithm 1: TRAVERSALORDER to improve size

Input: neural network f and input \mathbf{x}
Parameter : ϵ -perturbation
Output: traversal order π

```
1 function TRAVERSALORDER( $f, \mathbf{x}$ )
2    $c \mapsto f(\mathbf{x})$ 
3    $\hat{\mathbf{x}} \mapsto \text{newVars}()$ 
4   for  $x_i \in \mathbf{x}$  do
5      $\hat{x}_i \mapsto [x_i - \epsilon, x_i + \epsilon]$ 
6      $\hat{x}_j \mapsto [x_j, x_j]$  where  $j \neq i$ 
7     lower  $\mapsto \text{COMPUTEBOUND}(f, \hat{\mathbf{x}})$ 
8      $\epsilon\text{-bounds}[i] \mapsto \text{lower}_c$ 
9    $\pi \mapsto \text{arg sort}(\epsilon\text{-bounds, descending})$ 
10  return  $\pi$ 
```

Then, for each individual feature x_i in \mathbf{x} , we set a constraint on its corresponding variable \hat{x}_i , requiring it to be in the *interval* $[x_i - \epsilon, x_i + \epsilon]$ (Line 5). Each of the remaining feature variables \hat{x}_j , with $j \neq i$ and $j \in \{1, \dots, m\}$, is constrained to be equal to its corresponding input x_j (Line 6).¹ In Line 7, we pass $\hat{\mathbf{x}}$ (with only its i -th feature \hat{x}_i allowed to change) and the model f to a bounds-analysis procedure, which computes lower and upper bounds on the outputs of $f(\hat{\mathbf{x}})$. In particular, we obtain $\text{lower}_c \leq y_c \leq \text{upper}_c$ for the predicted output class $c \in C$. Note that, since f could be highly non-linear, computing these bounds is not straightforward. That is why, instead of performing simple model inferences, we utilize existing analyses such as IBP (interval bounded propagation) (Gowal et al. 2019) and CROWN (Zhang et al. 2018) to compute the output bounds. We found (empirically) that retaining only the lower bound of the predicted class lower_c provides the most effective ranking. We store the lower bound in Line 8. A for-loop is used to compute bounds for all the input features. We remark that the for-loop is only used to present the functionality in a clear way; in our implementation, all of the ϵ -bounds are computed in *parallel*. Once we have all the bounds, we sort them in a descending order (Line 9) – as input features producing higher lower bounds are more likely to be irrelevant to the explanation. Traversing less relevant features first leads to smaller explanations.

3.2 Improving time: a binary search-based traversal

Given a traversal order, the algorithm of (Wu, Wu, and Barrett 2023) simply processes the features one by one in a sequential order. Here, we propose an improvement that processes the features using an alternative approach inspired by binary search. The new algorithm searches for *batches* of *consecutive* irrelevant features. It simultaneously checks the whole batch to see whether it is irrelevant. If so, there is no need to process the features in the batch one by one. We note that this approach does not change the traversal order, so the computed explanation is the same as that computed by the original sequential algorithm.

¹As a further optimization (not shown), if the input data are known to be bounded as part of the problem definition, we intersect the interval $[x_i - \epsilon, x_i + \epsilon]$ with the known bound.

Algorithm 2: BINARYSEQUENTIAL to reduce time

Input: neural network f and input \mathbf{x}
Parameter : ϵ -perturbation, norm p
Output: explanation \mathbf{x}_A and irrelevant set \mathbf{x}_B

```
1  $\mathbf{x}_A, \mathbf{x}_B \mapsto \emptyset, \emptyset$ 
2  $\mathbf{x}_A, \mathbf{x}_B \mapsto \text{BINARYSEQUENTIAL}(f, \mathbf{x})$ 
3 function BINARYSEQUENTIAL( $f, \mathbf{x}_\Theta$ )
4   if  $|\mathbf{x}_\Theta| = 1$  then
5     if CHECK( $f, \mathbf{x}, \mathbf{x}_B \cup \mathbf{x}_\Theta$ ) then
6        $\mathbf{x}_B \mapsto \mathbf{x}_B \cup \mathbf{x}_\Theta$ 
7       return
8     else
9        $\mathbf{x}_A \mapsto \mathbf{x}_A \cup \mathbf{x}_\Theta$ 
10    return
11   $\mathbf{x}_\Phi, \mathbf{x}_\Psi = \text{split}(\mathbf{x}_\Theta, 2)$ 
12  if CHECK( $f, \mathbf{x}, \mathbf{x}_B \cup \mathbf{x}_\Phi$ ) then
13     $\mathbf{x}_B \mapsto \mathbf{x}_B \cup \mathbf{x}_\Phi$ 
14    if CHECK( $f, \mathbf{x}, \mathbf{x}_B \cup \mathbf{x}_\Psi$ ) then
15       $\mathbf{x}_B \mapsto \mathbf{x}_B \cup \mathbf{x}_\Psi$ 
16    else
17      if  $|\mathbf{x}_\Psi| = 1$  then
18         $\mathbf{x}_A \mapsto \mathbf{x}_A \cup \mathbf{x}_\Psi$ 
19      else
20        BINARYSEQUENTIAL( $f, \mathbf{x}_\Psi$ )
21  else
22    if  $|\mathbf{x}_\Phi| = 1$  then
23       $\mathbf{x}_A \mapsto \mathbf{x}_A \cup \mathbf{x}_\Phi$ 
24    else
25      BINARYSEQUENTIAL( $f, \mathbf{x}_\Phi$ )
26  BINARYSEQUENTIAL( $f, \mathbf{x}_\Psi$ )
```

In Algorithm 2, the procedure globally updates the explanation set \mathbf{x}_A and the irrelevant set \mathbf{x}_B throughout. To start with, these two sets are initialized to \emptyset . After executing $\text{BINARYSEQUENTIAL}(f, \mathbf{x})$, the input \mathbf{x} is partitioned into disjoint \mathbf{x}_A and \mathbf{x}_B , i.e., $\mathbf{x}_A \cup \mathbf{x}_B = \mathbf{x}$. In function $\text{BINARYSEQUENTIAL}(f, \mathbf{x}_\Theta)$, where \mathbf{x}_Θ are candidate features, the first if condition (Lines 4-10) considers the base case when there is only a single feature left in \mathbf{x}_Θ . If $\text{CHECK}(f, \mathbf{x}, \mathbf{x}_B \cup \mathbf{x}_\Theta)$ returns True (Line 5), i.e., perturbing the current \mathbf{x}_B and \mathbf{x}_Θ does not change model’s decision (same c for classification or $|c - c'| \leq \delta$ for regression), then \mathbf{x}_Θ is put into the irrelevant set \mathbf{x}_B (Line 6). Otherwise, it is added to the explanation set \mathbf{x}_A (Line 9). In the non-base case, \mathbf{x}_Θ has more than just one feature. For this case, we split \mathbf{x}_Θ into two sets \mathbf{x}_Φ and \mathbf{x}_Ψ with similar sizes (Line 11). If $\text{CHECK}(f, \mathbf{x}, \mathbf{x}_B \cup \mathbf{x}_\Phi)$ returns True (Line 12-20), then \mathbf{x}_Φ belongs to the irrelevant set \mathbf{x}_B (Line 13) and the procedure continues by checking if \mathbf{x}_Ψ is irrelevant (Line 14): if True, \mathbf{x}_Ψ is also added to \mathbf{x}_B (Line 15). Otherwise, if \mathbf{x}_Ψ contains only one feature (Line 17), we know it must be part of the explanation features and directly add it to \mathbf{x}_A (Line 18). (Note that this check avoids unnecessary execution of the very first if condition (Lines 4-10).) If not, we recursively call $\text{BINARYSEQUENTIAL}(f, \mathbf{x}_\Psi)$ to search for batches of consecutive irrelevant features in \mathbf{x}_Ψ (Line 20). Finally, if $\text{CHECK}(f, \mathbf{x}, \mathbf{x}_B \cup \mathbf{x}_\Phi)$ (Line 12) returns False (Lines 21-26), we similarly process \mathbf{x}_Φ . And when \mathbf{x}_Φ is done, we call

Algorithm 3: CHECK with confidence ranking

Input: network f , input \mathbf{x} , candidate features \mathbf{x}_Θ
Parameter: ϵ -perturbation
Output: True/False

```
1 function CHECK( $f, \mathbf{x}, \mathbf{x}_\Theta$ )
2    $\hat{\mathbf{x}}, \hat{\mathbf{y}} \mapsto \text{newVars}()$ 
3    $c, \mathbf{y} \mapsto f(\mathbf{x})$ 
4   ranking  $\mapsto \text{arg sort}(\mathbf{y}, \text{descending})$ 
5   for  $i \in \Theta$  do
6      $\phi \mapsto (\|\hat{x}_i - x_i\|_p \leq \epsilon)$ 
7   for  $i \in \Theta(\mathbf{x}) \setminus \Theta$  do
8      $\phi \mapsto \phi \wedge (\hat{x}_i = x_i)$ 
9   for  $j \in \text{ranking} \setminus c$  do
10    exitCode  $\mapsto \text{SOLVE}(f, \phi \Rightarrow \hat{y}_c < \hat{y}_j)$ 
11    if exitCode == UNSAT then
12      continue
13    else
14      break
15  return exitCode == UNSAT
```

BINARYSEQUENTIAL(f, \mathbf{x}_Ψ) to process \mathbf{x}_Ψ (Line 26).

Theorem 3.1 (Time Complexity). *Given a network f and an input $\mathbf{x} = \langle x_1, \dots, x_m \rangle$ where $m \geq 2$, the time complexity of BINARYSEQUENTIAL(f, \mathbf{x}) is 2 calls of CHECK for the best case (all features are irrelevant) and $k_{2m} = 2 \cdot k_m + 1$ or $k_{2m+1} = k_{m+1} + k_m + 1$ calls of CHECK for the worst case (all features are in explanation). When $m = 1$, it is obvious that it needs 1 CHECK call. Proof is in Appendix A.1.*

3.3 Improving time: introducing a confidence ranking

The CHECK procedure checks whether a model’s decision is invariant under ϵ -perturbations of a specified subset of input features. That is, it must check whether the output c is in an allowable range for regression, i.e., $|c - c'| \leq \delta$, or whether the confidence of the predicted class y_c is always the greatest among all classes, i.e., $y_c = \max(\mathbf{y})$. In the latter case, this means that in the worst case, $|\mathbf{y}| - 1$ separate checks are needed to ensure that y_c is the largest. In previous work (Wu, Wu, and Barrett 2023), these checks are done naively without any insight into what order should be used. In this work, we propose *ranking* these checks based on the confidence values of the corresponding outputs. We then proceed to do the checks from the *most* to the *least* likely classes. If a check fails, i.e., invariance of the model prediction is not guaranteed, this is typically because we can perturb the inputs to produce one of the next most likely classes. Thus, by checking the most likely classes first, we avoid the need for additional checks if one of those checks already fails.

Algorithm 3 shows the CHECK procedure which checks whether imposing ϵ -perturbations on certain features \mathbf{x}_Θ of input \mathbf{x} maintains the decision of model f : if yes, it returns True, meaning that these features are irrelevant. To start with, we use variables $\hat{\mathbf{x}}$ and $\hat{\mathbf{y}}$ to represent the inputs and outputs of the model and set \mathbf{y} to be the logits and c to be the predicted class. In Line 4, we rank the confidence values of all the classes in a descending order. In other words, we prioritize the

classes that are most likely after c . We allow ϵ -perturbation on features in \mathbf{x}_Θ while fixing the others (Lines 5–8). For each class j in the sorted ranking (excluding c as this is the predicted class to be compared with), we call SOLVE to examine whether the specification $\phi \Rightarrow \hat{y}_c < \hat{y}_j$ holds, i.e., whether the input constraints ϕ allow a prediction change with \hat{y}_c smaller than \hat{y}_j (Line 10). If the exitCode of SOLVE is UNSAT, then it means the specification is unsatisfiable in the sense that \hat{y}_c will always be greater than or equal to \hat{y}_j , i.e., the prediction cannot be manipulated into class j . The for loop (Lines 9–14) examines each class in ranking $\setminus c$, and if all checks are UNSAT (algorithm returns True in Line 15), then \hat{y}_c is ensured to be the greatest among $\hat{\mathbf{y}}$, i.e., prediction invariance is guaranteed. Otherwise, if SOLVE returns SAT or Unknown for any \hat{y}_j , the algorithm returns False. The key insight is that SOLVE is more likely to return SAT for classes with higher confidence, and once it does, the algorithm terminates. In practice, SOLVE can be instantiated with off-the-shelf neural network verification tools (Singh et al. 2019; Müller et al. 2022; Katz et al. 2019; Wang et al. 2021; Henriksen and Lomuscio 2020; Wu et al. 2024).

3.4 A trade-off between size and time: QUICKXPLAIN

In previous sections, we propose approaches to orthogonally improve explanation size and generation time; in this section, we adapt the QuickXplain algorithm (Junker 2004) and optimize such adaptation (Huang and Marques-Silva 2023) to provide an additional *trade-off* between these two metrics. We remark that the QuickXplain-based approach works as an alternative to the binary search-based method, i.e., given a traversal order from the first step of our workflow, we can either use binary search or QuickXplain. The former improves time but does not affect size, whereas the latter affects both. In practice QuickXplain tends to produce smaller explanations but requires more time to do so. Confidence ranking benefits both techniques as it accelerates CHECK.

We present our QUICKXPLAIN adaptation in Algorithm 4. The function QXP($\mathbf{x}_\alpha, \mathbf{x}_\beta, \mathbf{x}_\Theta$) itself is recursive with three arguments: (1) the current explanation \mathbf{x}_α ; (2) the current irrelevant set \mathbf{x}_β ; and (3) the current (sub)set of input features that need to be analyzed, \mathbf{x}_Θ . These three sets always form a partition of the full set of features. To start with, \mathbf{x}_α and \mathbf{x}_β are initialized to \emptyset , and when QXP proceeds, irrelevant features are added into \mathbf{x}_β in a monotonically increasing way; finally, after all features are done, \mathbf{x}_α is returned as the optimal explanation \mathbf{x}_A and \mathbf{x}_β as the irrelevant set \mathbf{x}_B . Now we walk through the algorithm. Lines 3–7 considers the base case when \mathbf{x}_Θ has a single feature as in Algorithm 2. When there are more than one feature in \mathbf{x}_Θ , it is split into two subsets \mathbf{x}_Φ and \mathbf{x}_Ψ (Line 8). In Lines 9–12, we check if the subset \mathbf{x}_Φ or \mathbf{x}_Ψ belongs to the irrelevant set: if True, then we add it into \mathbf{x}_β when calling QXP to process the other subset. If neither \mathbf{x}_Φ nor \mathbf{x}_Ψ is irrelevant, we take turns to process \mathbf{x}_Φ and \mathbf{x}_Ψ in Lines 13–22: the first if condition analyzes \mathbf{x}_Φ and the second if processes \mathbf{x}_Ψ . If either of them has a single feature, then they are regarded as an explanation feature \mathbf{x}'_Φ (Line 15) or \mathbf{x}'_Ψ (Line 19) directly. This is to avoid the unnecessary execution of the very first if condition

Algorithm 4: QUICKXPLAIN to provide a trade-off

Input: neural network f and input \mathbf{x} **Parameter:** ϵ -perturbation, norm p **Output:** explanation \mathbf{x}_A and irrelevant set \mathbf{x}_B

```

1  $\mathbf{x}_A, \mathbf{x}_B \mapsto \text{QXP}(\emptyset, \emptyset, \mathbf{x})$ 
2 function QXP( $\mathbf{x}_\alpha, \mathbf{x}_\beta, \mathbf{x}_\Theta$ )
3   if  $|\mathbf{x}_\Theta| = 1$  then
4     if CHECK( $f, \mathbf{x}, \mathbf{x}_\beta \cup \mathbf{x}_\Theta$ ) then
5       return  $\emptyset, \mathbf{x}_\beta \cup \mathbf{x}_\Theta$ 
6     else
7       return  $\mathbf{x}_\Theta, \mathbf{x}_\beta$ 
8    $\mathbf{x}_\Phi, \mathbf{x}_\Psi = \text{split}(\mathbf{x}_\Theta, 2)$ 
9   if CHECK( $f, \mathbf{x}, \mathbf{x}_\beta \cup \mathbf{x}_\Phi$ ) then
10    return QXP( $\mathbf{x}_\alpha, \mathbf{x}_\beta \cup \mathbf{x}_\Phi, \mathbf{x}_\Psi$ )
11  else if CHECK( $f, \mathbf{x}, \mathbf{x}_\beta \cup \mathbf{x}_\Psi$ ) then
12    return QXP( $\mathbf{x}_\alpha, \mathbf{x}_\beta \cup \mathbf{x}_\Psi, \mathbf{x}_\Phi$ )
13  else
14    if  $|\mathbf{x}_\Phi| = 1$  then
15       $\mathbf{x}'_\Phi, \mathbf{x}'_\beta \mapsto \mathbf{x}_\Phi, \mathbf{x}_\beta$ 
16    else
17       $\mathbf{x}'_\Phi, \mathbf{x}'_\beta \mapsto \text{QXP}(\mathbf{x}_\alpha \cup \mathbf{x}_\Psi, \mathbf{x}_\beta, \mathbf{x}_\Phi)$ 
18    if  $|\mathbf{x}_\Psi| = 1$  then
19       $\mathbf{x}''_\Psi, \mathbf{x}''_\beta \mapsto \mathbf{x}_\Psi, \mathbf{x}'_\beta$ 
20    else
21       $\mathbf{x}''_\Psi, \mathbf{x}''_\beta \mapsto \text{QXP}(\mathbf{x}_\alpha \cup \mathbf{x}'_\Phi, \mathbf{x}'_\beta, \mathbf{x}_\Psi)$ 
22    return  $\mathbf{x}'_\Phi \cup \mathbf{x}''_\Psi, \mathbf{x}''_\beta$ 

```

(Lines 3–7) in the new instance of calling QXP since we already know they are not irrelevant.² If both of them have more than one feature, then QXP is called to process them separately: \mathbf{x}_Φ is processed in Line 17 with \mathbf{x}_Ψ as part of the new \mathbf{x}_α , and \mathbf{x}_Ψ is processed in Line 21 with \mathbf{x}'_Φ as part of the new \mathbf{x}_α . Finally, both \mathbf{x}'_Φ and \mathbf{x}''_Ψ are returned as explanation features, and \mathbf{x}''_β is returned as the irrelevant set (Line 22).

Theorem 3.2 (Time Complexity). *Give a neural network f and an input $\mathbf{x} = \langle x_1, \dots, x_m \rangle$ where $m \geq 2$, the time complexity of $\text{QXP}(\emptyset, \emptyset, \mathbf{x})$ is $\lfloor \log_2 m \rfloor + 1$ calls of CHECK for the best case (all features are irrelevant) and $(m - 1) \times 2$ calls of CHECK for the worst case (all features are in explanation). When $m = 1$, it is obvious that it needs 1 CHECK call. Proof is in Appendix A.2.*

4 Experimental results

We have implemented the VERIX+ framework in Python. To realize the COMPUTEBOUND analysis in Algorithm 1, we utilize the bound-propagation³ package for fully-connected models and the auto_LiRPA⁴ library for convolutional models. While the latter also supports dense layers, the former computes tighter IBP bounds which, in our case, lead to smaller explanations. We use Marabou⁵, a neural network ver-

²This enables Algorithm 4 calling fewer numbers of the CHECK procedure (i.e., fewer oracle calls) than the similar adaptation of QuickXplain in (Huang and Marques-Silva 2023).

³<https://pypi.org/project/bound-propagation/>

⁴https://github.com/Verified-Intelligence/auto_LiRPA

⁵<https://github.com/NeuralNetworkVerification/Marabou>

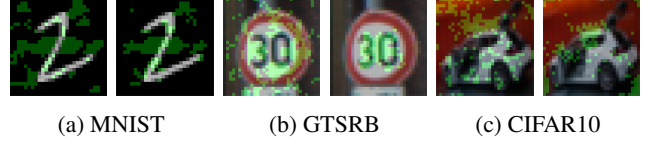


Figure 2: Comparison between VERIX (left) and VERIX+ (right) explanations for different datasets. (a) MNIST-CNN: size 187 vs. 137, and time 635 vs. 51. (b) CIFAR10-FC: size 208 vs. 146, and time 482 vs. 57. (c) GTSRB-FC: size 276 vs. 117, and time 703 vs. 49.

ification tool, to perform the SOLVE function in Algorithm 3. Our framework can accommodate other existing tools as long as they can perform the COMPUTEBOUND or the SOLVE functionality. We trained networks on standard image benchmarks such as the MNIST (LeCun, Cortes, and Burges 2010), GTSRB (Stallkamp et al. 2012), and CIFAR10 (Krizhevsky et al. 2009) datasets with model structures in Appendix C.1.

4.1 Improvements for explanation size and generation time

We report on improvements to explanation *size* and generation *time* in Table 1, accompanied with example explanations in Figure 2. For each data point in the table, we collect “valid” explanations (i.e., excluding examples that are robust to ϵ -perturbation) for the first 100 test images (to avoid selection bias) and take the average time and size. Experiments were performed on a workstation equipped with 16 AMD Ryzen™ 7 5700G CPUs and 32GB memory running Fedora 37.

From the MNIST-FC data points highlighted in yellow, we observe that probability ranking decreases *time* from 92.3 to 81.4, and binary search-based traversal further reduces it to 29.6. Similarly, for MNIST-CNN, *time* is significantly reduced from the original 439.2 to 46.3. Moreover, applying bound propagation-based traversal ultimately reduces time to 28.4 and 42.0 (~ 10 times faster) accordingly, as it adjusts the traversal order during computation and thus affects time and size simultaneously. That said, on MNIST-CNN, VERIX+ achieves 90.43% reduction in *time* over VERIX. We notice that size reduction on MNIST is not significant. We speculate that this is because the explanations obtained using the original approach (Wu, Wu, and Barrett 2023) are already close to the global optima, so there is little room for improvement. We show an example explanation for the MNIST-CNN model in Figure 2a. For the digit “2”, we can see that both explanations focus on the central region as intuitively turning these pixels from black into white may change the prediction into “8”. In comparison, VERIX+ reduces both size and time.

On the other hand, *size* reduction is more substantial on GTSRB and CIFAR10, as shown by the data points in blue. For instance, using heuristic sensitivity on GTSRB-FC, binary search-based traversal has size 529.4 with a reduction of time from 614.9 to 233.8. When deploying QuickXplain, *size* is reduced to 485.0 with a slight overhead, i.e., a trade-off between size and time. Meanwhile, applying bound propagation-based traversal further reduces *size* to 333.4. Similarly, for GTSRB-CNN, *size* decreases from 569.0 to 355.3, i.e., an overall reduction of 37.56%. As for CIFAR10-FC, *size* is reduced from 588.9 to 465.8 when applying bound

Table 1: Improvements of VERIX+ on average explanation size (number of pixels) and generation time (seconds) under combinatorial configurations for fully-connected (-FC) and convolutional (-CNN) models trained on standard image benchmarks. ϵ is set to 5%, 1%, and 1% for the MNIST, GTSRB, and CIFAR10 datasets, respectively.

traversal order search procedure metrics	VERIX		VERIX+											
	heuristic		heuristic						bound propagation					
	sequential		prob ranking		binary search		QuickXplain		prob ranking		binary search		QuickXplain	
size	time	size	time	size	time	size	time	size	time	size	time	size	time	
MNIST-FC	186.7	92.3	186.7	81.4	186.7	29.6	186.3	32.1	179.5	70.6	179.5	28.4	179.0	32.2
MNIST-CNN	105.7	439.2	105.7	398.9	105.7	46.3	105.7	51.5	100.8	295.8	100.8	42.0	100.6	47.4
GTSRB-FC	529.4	614.9	529.4	488.0	529.4	233.8	485.0	286.6	333.6	437.7	333.6	149.7	333.4	196.1
GTSRB-CNN	569.0	1897.6	569.0	1312.7	569.0	394.0	506.0	466.4	355.8	1430.8	355.8	251.0	355.3	330.1
CIFAR10-FC	588.9	438.0	588.9	357.7	588.9	292.2	582.4	383.5	465.8	354.9	465.8	238.8	465.7	316.9
CIFAR10-CNN	664.8	1617.0	664.8	1033.5	664.8	448.2	652.9	567.8	553.5	1152.8	553.5	371.1	552.8	482.2

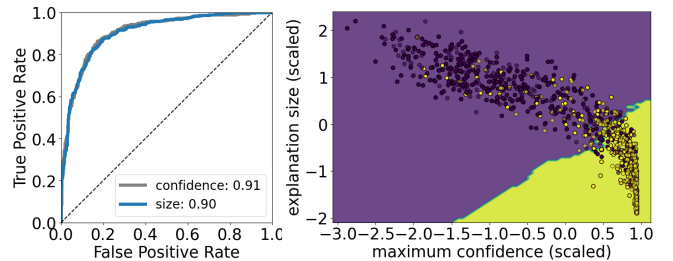
Table 2: Comparing VERIX+ explanation sizes (number of pixels) for normally and adversarially trained MNIST-FC models. ϵ is set to 5%, and ϵ -robust denotes the percentage of ϵ -robust samples.

samples	MNIST-FC				MNIST-FC-ADV					
	accuracy	correct ϵ -robust	size	incorrect ϵ -robust	size	accuracy	correct ϵ -robust	size	incorrect ϵ -robust	size
original	93.76%	4%	177.20	0.3%	398.85	92.85%	52.3%	128.22	2%	311.14
malicious	23.66%	0%	466.30	0%	562.07	82.66%	6.7%	298.57	0.3%	536.41

propagation-based traversal, and time is further reduced to 238.8 with binary search. In Figure 2b, we show an example explanation from GTSRB. For the traffic sign “30 mph”, the explanation from VERIX+ makes more sense as it focuses on the central region, particularly “30”, whereas the baseline is largely scattered around the background. For this image, we have size reduced by 57.6% and time reduced by 93.0%.

4.2 Explanations for normally and adversarially trained models

In Table 2, we compare our explanations for normally and adversarially trained MNIST-FC models on original and malicious samples. We describe the adversarial training for the MNIST-FC-ADV model in Appendix C.2. We produce explanations for both correct and incorrect samples. For each data point, we collected 300 samples and reported their average explanation size (excluding ϵ -robust samples). Overall, we observe that both models have smaller explanations for original samples over malicious ones, and for correct predictions over incorrect ones. In comparison, the adversarially trained MNIST-FC-ADV model produces smaller explanations than MNIST-FC under all conditions. For instance, for the original and correct samples, MNIST-FC-ADV produces 27.64% smaller explanations than its normal counterpart (128.22 vs. 177.20). This is expected since with adversarial training, the model learns more implicit information about the samples, e.g., which pixels likely contain the key information for prediction and which are trivial perturbations, and thus only needs to pay attention to fewer yet indispensable pixels to make a correct decision. In Figure 10 of Appendix C.2, we show examples when MNIST-FC-ADV produces smaller explanations for both original and malicious inputs. This is also reflected in the ϵ -robust rate, which increases from 4% to 52.3% after adversarial training, since now the model has learned to capture these principal features in the input and



(a) MNIST: AUROC (b) MNIST: A KNN classifier

Figure 3: Detecting incorrect examples for MNIST. (a) ROC curves and AUROC values. (b) A KNN classifier.

become less sensitive to perturbations.

4.3 Using explanation size to detect incorrect predictions

We demonstrate that explanation size is a useful proxy for detecting incorrect examples. Specifically, we collected 1000 samples – 500 correctly and 500 incorrectly classified – for both MNIST and GTSRB, and present our analysis in Figures 3 and 6 of Appendix B.1. For MNIST, Figure 5 of Appendix B.1 shows that there exists a significant separation between the correct and incorrect clusters. Previously, (Hendrycks and Gimpel 2017) proposed using the maximum softmax probabilities to detect erroneously classified examples. Following this, in Figures 3a and 6c, we plot the receiver operating characteristic (ROC) curves and compute the AUROC (area under the ROC curve) values when using maximum confidence (gray) and explanation size (blue) independently. We observe that our explanation size has a competitive effect on both datasets. Furthermore, utilizing both confidence and size, we trained classifiers to detect whether the prediction of an unseen sample is correct or er-

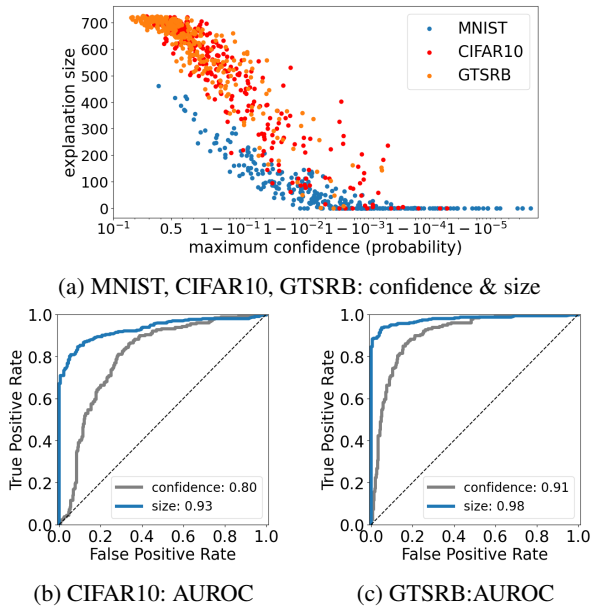


Figure 4: Detecting *out-of-distribution* examples from CIFAR10 and GTSRB for the MNIST-CNN model. (a) Explanation size and maximum confidence (*log scale*, see *linear scale* in Figure 8a). (b)(c) ROC curves and AUROC values for OOD samples from CIFAR10 and GTSRB, respectively.

roneous. We split the 1000 samples into a training set (700 samples) and a test set (300 samples), and then trained a k -nearest neighbor (KNN) classifier for each dataset. As in Figures 3b and 6b, these two classifiers achieve 82% and 73% accuracy, respectively. Without loss of generosity, in Figure 7 of Appendix B.1, we also trained various other classifiers, including neural networks, support vector machines, and decision trees, and observe that they achieve similar accuracies.

4.4 Using explanation size to detect out-of-distribution examples

We also show that explanation size can help detect *out-of-distribution* (OOD) samples. Consider the scenario in which CIFAR10 and GTSRB images are fed into the MNIST-CNN model as OOD samples (we crop the former two to let them have the same size as MNIST). We use the OpenCV library to convert color images into gray-scale. The goal is to preserve the primary semantic meanings at the center of these images. We collected 900 samples in total – 300 each from MNIST, CIFAR10, and GTSRB, and plotted their maximum softmax probability and explanation size, as shown in Figures 4a and 8a of Appendix B.2. We observe a significant separation between the in- and out-of-distribution samples. The existing work (Hendrycks and Gimpel 2017) mentioned above used the maximum softmax probabilities for OOD detection also. Following this, we compare the effect of using maximum confidence and explanation size to detect OOD samples from CIFAR10 and GTSRB. From Figures 4b and 4c, we can see that explanation size yields better ROC curves for both datasets and also achieves higher AUROC values, i.e., 93% on CIFAR10 and 98% on GTSRB. We perform similar OOD detection on the MNIST-FC model, and show the advantages

of using explanation size in Figure 9 of Appendix B.2.

5 Related work

Several approaches to formal explanations (Marques-Silva and Ignatiev 2022) have been explored in the past. (Ignatiev, Narodytska, and Marques-Silva 2019) first proposed using abductive reasoning to compute formal explanations for neural networks by encoding them into a set of constraints and then deploying automated reasoning systems such as Satisfiability Modulo Theories (SMT) solvers to solve the constraints. (La Malfa et al. 2021) brings in bounded perturbations, k -nearest neighbors and ϵ -balls to produce distance-restricted explanations for natural language models. Adapting the ϵ -perturbations to perception models for which inputs tend to be naturally bounded, (Wu, Wu, and Barrett 2023) proposes a feature-level sensitivity heuristic to obtain a ranking of the input features and thus produce empirically small explanations. In this paper, we utilize bound propagation-based techniques to obtain more fine-grained feature-level sensitivity. Compared to the existing heuristic from (Wu, Wu, and Barrett 2023) and later adopted by (Izza et al. 2024), we obtain ϵ -perturbation dependent traversal orders that lead to even smaller explanation sizes. To reduce generation time, (Huang and Marques-Silva 2023) mimics the QuickXplain algorithm (Junker 2004) to avoid traversing all the features in a linear way (experiments only include the linear case though). Our optimization of this QuickXplain adaptation further reduces the number of oracle calls; we also perform a complete experimental comparison between the linear and non-linear approaches. Additionally, we introduce binary search-based traversals to further improve time. The Dichotomic search method from (Izza et al. 2024) is also inspired by binary search, but it includes unnecessary oracle calls, as it searches from the beginning every time after it finds a “transition feature.” Therefore, as the authors say in the paper, in their experiments, the number of oracle calls needed by their Dichotomic search is “always larger than” the number of input features. In contrast, our recursive binary search-based algorithm does not have such redundant oracle calls and thus achieves much reduced generation time. Finally, our confidence ranking strategy accelerates the CHECK procedure, which benefits all such oracle calls. To the best of our knowledge, this is the first time that this strategy is proposed.

6 Conclusion and future work

We have presented the VERIX+ framework for computing optimal verified explanations with improved *size* and generation *time*. We also demonstrated the usefulness of the generated explanations in detecting incorrect and out-of-distribution examples. Future work could explore further techniques for improving the performance of verified explanation generation, perhaps by adapting parallel techniques from (Izza et al. 2024) or by finding ways to introduce approximations in order to gain scalability. It would also be interesting to evaluate explanations on other metrics such as usefulness to humans rather than simply size. Finally, we would like to explore additional applications, especially in areas where safety or fairness is crucial.

References

- Darwiche, A.; and Hirth, A. 2020. On the reasons behind decisions. In *Proceedings of the 24th European Conference on Artificial Intelligence*.
- Goodfellow, I. J.; Shlens, J.; and Szegedy, C. 2014. Explaining and harnessing adversarial examples. *arXiv preprint arXiv:1412.6572*.
- Gowal, S.; Dvijotham, K. D.; Stanforth, R.; Bunel, R.; Qin, C.; Uesato, J.; Arandjelovic, R.; Mann, T.; and Kohli, P. 2019. Scalable verified training for provably robust image classification. In *Proceedings of the IEEE/CVF International Conference on Computer Vision*, 4842–4851.
- Guo, C.; Pleiss, G.; Sun, Y.; and Weinberger, K. Q. 2017. On calibration of modern neural networks. In *International conference on machine learning*, 1321–1330. PMLR.
- Hein, M.; Andriushchenko, M.; and Bitterwolf, J. 2019. Why ReLU Networks Yield High-Confidence Predictions Far Away From the Training Data and How to Mitigate the Problem. 41–50.
- Hendrycks, D.; and Gimpel, K. 2017. A Baseline for Detecting Misclassified and Out-of-Distribution Examples in Neural Networks. In *International Conference on Learning Representations*.
- Henriksen, P.; and Lomuscio, A. 2020. Efficient neural network verification via adaptive refinement and adversarial search. In *ECAI 2020*, 2513–2520. IOS Press.
- Huang, X.; and Marques-Silva, J. 2023. From robustness to explainability and back again. *arXiv preprint arXiv:2306.03048*.
- Ignatiev, A.; Narodytska, N.; and Marques-Silva, J. 2019. Abduction-based explanations for machine learning models. In *Proceedings of the AAAI Conference on Artificial Intelligence*, 1511–1519.
- Izza, Y.; Huang, X.; Morgado, A.; Planes, J.; Ignatiev, A.; and Marques-Silva, J. 2024. Distance-Restricted Explanations: Theoretical Underpinnings & Efficient Implementation. *arXiv preprint arXiv:2405.08297*.
- Junker, U. 2004. Quickxplain: Preferred explanations and relaxations for over-constrained problems. In *Proceedings of the 19th national conference on Artificial intelligence*, 167–172.
- Katz, G.; Huang, D. A.; Ibeling, D.; Julian, K.; Lazarus, C.; Lim, R.; Shah, P.; Thakoor, S.; Wu, H.; Zeljić, A.; et al. 2019. The marabou framework for verification and analysis of deep neural networks. In *International Conference on Computer Aided Verification*, 443–452.
- Krizhevsky, A.; et al. 2009. Learning multiple layers of features from tiny images. Technical report.
- La Malfa, E.; Michelmoro, R.; Zbrzezny, A. M.; Paoletti, N.; and Kwiatkowska, M. 2021. On Guaranteed Optimal Robust Explanations for NLP Models. In Zhou, Z.-H., ed., *Proceedings of the Thirtieth International Joint Conference on Artificial Intelligence, IJCAI-21*, 2658–2665.
- LeCun, Y.; Cortes, C.; and Burges, C. 2010. MNIST handwritten digit database. *ATT Labs [Online]*. Available: <http://yann.lecun.com/exdb/mnist, 2>.
- Lundberg, S. M.; and Lee, S.-I. 2017. A unified approach to interpreting model predictions. In *Proceedings of the 31st International Conference on Neural Information Processing Systems*, 4768–4777.
- Marques-Silva, J.; and Ignatiev, A. 2022. Delivering Trustworthy AI through formal XAI. In *Proceedings of the AAAI Conference on Artificial Intelligence*, 3806–3814.
- Müller, M. N.; Makarchuk, G.; Singh, G.; Püschel, M.; and Vechev, M. 2022. PRIMA: general and precise neural network certification via scalable convex hull approximations. *Proceedings of the ACM on Programming Languages*, 6(POPL): 1–33.
- Ribeiro, M. T.; Singh, S.; and Guestrin, C. 2016. “Why should i trust you?” Explaining the predictions of any classifier. In *Proceedings of the 22nd ACM SIGKDD international conference on knowledge discovery and data mining*, 1135–1144.
- Ribeiro, M. T.; Singh, S.; and Guestrin, C. 2018. Anchors: high-precision model-agnostic explanations. In *Proceedings of the Thirty-Second AAAI Conference on Artificial Intelligence and Thirtieth Innovative Applications of Artificial Intelligence Conference and Eighth AAAI Symposium on Educational Advances in Artificial Intelligence*, 1527–1535.
- Shih, A.; Choi, A.; and Darwiche, A. 2018. A symbolic approach to explaining Bayesian network classifiers. In *Proceedings of the 27th International Joint Conference on Artificial Intelligence*, 5103–5111.
- Singh, G.; Gehr, T.; Püschel, M.; and Vechev, M. 2019. An abstract domain for certifying neural networks. *Proceedings of the ACM on Programming Languages*, 3(POPL): 1–30.
- Stallkamp, J.; Schlipsing, M.; Salmen, J.; and Igel, C. 2012. Man vs. computer: Benchmarking machine learning algorithms for traffic sign recognition. *Neural networks*, 32: 323–332.
- Wang, S.; Zhang, H.; Xu, K.; Lin, X.; Jana, S.; Hsieh, C.-J.; and Kolter, Z. 2021. Beta-CROWN: Efficient Bound Propagation with Per-neuron Split Constraints for Neural Network Robustness Verification. In *Proceedings of the 35th Conference on Neural Information Processing Systems (NeurIPS)*, volume 34, 29909–29921.
- Wu, H.; Isac, O.; Zeljić, A.; Tagomori, T.; Daggitt, M.; Kokke, W.; Refaeli, I.; Amir, G.; Julian, K.; Bassan, S.; et al. 2024. Marabou 2.0: a versatile formal analyzer of neural networks. In *International Conference on Computer Aided Verification*, 249–264. Springer.
- Wu, M.; Wu, H.; and Barrett, C. 2023. VeriX: Towards Verified Explainability of Deep Neural Networks. In Oh, A.; Naumann, T.; Globerson, A.; Saenko, K.; Hardt, M.; and Levine, S., eds., *Advances in Neural Information Processing Systems*, volume 36, 22247–22268. Curran Associates, Inc.
- Zhang, H.; Weng, T.-W.; Chen, P.-Y.; Hsieh, C.-J.; and Daniel, L. 2018. Efficient neural network robustness certification with general activation functions. In *Proceedings of the 32nd International Conference on Neural Information Processing Systems*, 4944–4953.

A Proofs for theorems in Section 3

A.1 Proof for Theorem 3.1

Theorem 3.1 (Time Complexity). Given a network f and an input $\mathbf{x} = \langle x_1, \dots, x_m \rangle$ where $m \geq 2$, the *time complexity* of $\text{BINARYSEQUENTIAL}(f, \mathbf{x})$ is 2 calls of CHECK for the *best* case (all features are irrelevant) and $k_{2m} = 2 \cdot k_m + 1$ or $k_{2m+1} = k_{m+1} + k_m + 1$ calls of CHECK for the *worst* case (all features are in explanation). When $m = 1$, it is obvious that it needs 1 CHECK call.

Proof. It is straightforward that, when \mathbf{x} has a single feature, i.e., $m = 1$ and thus $|\mathbf{x}_\Theta| = 1$, only the first if condition of Algorithm 2 will be executed. That said, only 1 call of the CHECK procedure in Line 5 is needed.

For the non-base case, when there are more than one input features, i.e., $m \geq 2$, we analyze the time complexity of $\text{BINARYSEQUENTIAL}(f, \mathbf{x})$ for the *best* case and the *worst* case separately.

- In the *best* case, all the features are irrelevant so the input is essentially ϵ -robust. The original input \mathbf{x} is split into two subsets \mathbf{x}_Φ and \mathbf{x}_Ψ in Line 11. Algorithm 2 then terminates after two calls of CHECK in Lines 12 and 14 to examine whether \mathbf{x}_Φ and \mathbf{x}_Ψ are irrelevant, respectively. When CHECK returns True, they are put into the irrelevant set \mathbf{x}_B and the algorithm terminates. Therefore, for the best case, only 2 CHECK calls are needed.
- In the *worst* case, all the input features are relevant. That is, the whole input \mathbf{x} is an explanation. For this, we use k_m to denote the number of CHECK calls needed for an input that comprises m features, and use k_{2m} and k_{2m+1} to denote that of an input comprising even and odd features, respectively.

For an input \mathbf{x} that has $2m$ features (i.e., *even* features), when calling BINARYSEQUENTIAL , Line 11 splits it into two subsets \mathbf{x}_Φ and \mathbf{x}_Ψ , each of which has m features. Then, the algorithm runs the CHECK procedure in Line 12 to check if the first subset \mathbf{x}_Φ is irrelevant. It returns False as all features are relevant. Thus, the algorithm proceeds to the else condition in Line 21. Since \mathbf{x}_Φ has m features and $m \geq 2$, $\text{BINARYSEQUENTIAL}(f, \mathbf{x}_\Phi)$ in Line 25 is invoked. Afterwards, $\text{BINARYSEQUENTIAL}(f, \mathbf{x}_\Psi)$ is invoked to check the second subset \mathbf{x}_Ψ . Each such instantiation of BINARYSEQUENTIAL takes the worst case as the whole input is an explanation. Therefore, for an input comprising $2m$ features, it will need k_m CHECK calls for subset \mathbf{x}_Φ and k_m CHECK calls for subset \mathbf{x}_Ψ , as well as the extra 1 CHECK call in Line 21 at the beginning. That is, $k_{2m} = 2 \cdot k_m + 1$. This is the case when the input has even number of features.

Now if it has *odd* features, e.g., $2m + 1$, it will be split into two subsets with different sizes. In our case, when $|\mathbf{x}|$ is odd, we set $|\mathbf{x}_\Phi| = |\mathbf{x}_\Psi| + 1$. That is, the first subset \mathbf{x}_Φ has $m + 1$ features and the second subset \mathbf{x}_Ψ has m features. Similarly, the algorithm needs to run the 1 CHECK in Line 12, and then proceeds to work with \mathbf{x}_Φ and \mathbf{x}_Ψ accordingly. Therefore, for an input that consists of $2m + 1$ features, we have $k_{2m+1} = k_{m+1} + k_m + 1$.

□

A.2 Proof for Theorem 3.2

Theorem 3.2 (Time Complexity). Give a neural network f and an input $\mathbf{x} = \langle x_1, \dots, x_m \rangle$ where $m \geq 2$, the *time complexity* of $\text{QXP}(\emptyset, \emptyset, \mathbf{x})$ is $\lfloor \log_2 m \rfloor + 1$ calls of CHECK for the *best* case (all features are irrelevant) and $(m - 1) \times 2$ calls of CHECK for the *worst* case (all features are in explanation). When $m = 1$, it is obvious that it needs 1 CHECK call.

Proof. It is straightforward that, when \mathbf{x} has a single feature, i.e., $m = 1$ and thus $|\mathbf{x}_\Theta| = 1$, only the first if condition of Algorithm 4 will be executed. That said, only 1 call of the CHECK procedure in Line 3 is needed.

For the non-base case, when there are more than one input features, i.e., $m \geq 2$, we analyze the time complexity of $\text{QXP}(\emptyset, \emptyset, \mathbf{x})$ for the *best* case and the *worst* case separately.

- In the *best* case, all features are irrelevant so the input is essentially ϵ -robust. The original input \mathbf{x} is split into two subsets \mathbf{x}_Φ and \mathbf{x}_Ψ in Line 8. Then in Line 9 the CHECK procedure examines if the first subset \mathbf{x}_Φ is irrelevant. Since this is the best case when all features are irrelevant, it will return True. Then Line 10 will be executed to recursively call the QXP function to process the second subset \mathbf{x}_Ψ . In the new instantiation, similarly Lines 8, 9, and 10 will be executed so the QXP function is revoked again. This recursion continues until there is only one feature in the candidate feature set \mathbf{x}_Θ . Then in Line 4, the CHECK procedure examines the single feature, and the algorithm returns. That said, the number of CHECK calls is how many times the original input \mathbf{x} can be divided into two subsets until there is only one feature left, plus the final CHECK call to process the last single feature. In other words, it is the number of times we can divide m by 2 until we get 1, which is $\lfloor \log_2 m \rfloor$, plus the extra 1 call, hence $\lfloor \log_2 m \rfloor + 1$. Here, the floor function $\lfloor \cdot \rfloor$ is to accommodate the situation when $\log_2 m$ is not an integer, since we split \mathbf{x} as $|\mathbf{x}_\Phi| = |\mathbf{x}_\Psi| + 1$ when \mathbf{x} has odd features.
- In the *worst* case, all the input features are relevant. That is, the whole input \mathbf{x} is an explanation. After splitting \mathbf{x} into two subsets \mathbf{x}_Φ and \mathbf{x}_Ψ in Line 8, the CHECK procedure examines whether \mathbf{x}_Φ and \mathbf{x}_Ψ are irrelevant features in the if conditions in Lines 9 and 11, respectively. Both will return False as all input features are relevant for this case. Then the QXP function is recursively called to process the first subset \mathbf{x}_Φ in Line 17 and the second subset \mathbf{x}_Ψ in Line 21. These new instantiations will have similar executions as above, until eventually each subset contains only a single feature. Then, in Lines 15 and 19, subsets \mathbf{x}_Φ and \mathbf{x}_Ψ will be directly regarded as explanation features. Note that here we do not need another round of calling the QXP function, as we already know from Lines 9 and 11 that \mathbf{x}_Φ and \mathbf{x}_Ψ are not irrelevant thus in the explanation. That said, every time the candidate set \mathbf{x}_Θ is split into two subsets, two CHECK calls are needed for both subsets. Such division terminates when each input feature is in an individual subset. Since for an input \mathbf{x} that has m features, $m - 1$ divisions are needed, therefore the total number of CHECK calls is $(m - 1) \cdot 2$.

□

B Supplementary experimental results

B.1 Detecting incorrect examples

Modern neural networks have the tendency of being overly confident and making incorrect predictions with higher confidence compared to actual prediction accuracies (Guo et al. 2017; Hein, Andriushchenko, and Bitterwolf 2019). However, for safety-critical applications, we hope to ensure networks flag potentially incorrect predictions for human intervention. In addition to MNIST results presented in Figure 3 of Section 4.3, we additionally present GTSRB results in Figure 6 to illustrate generalization.

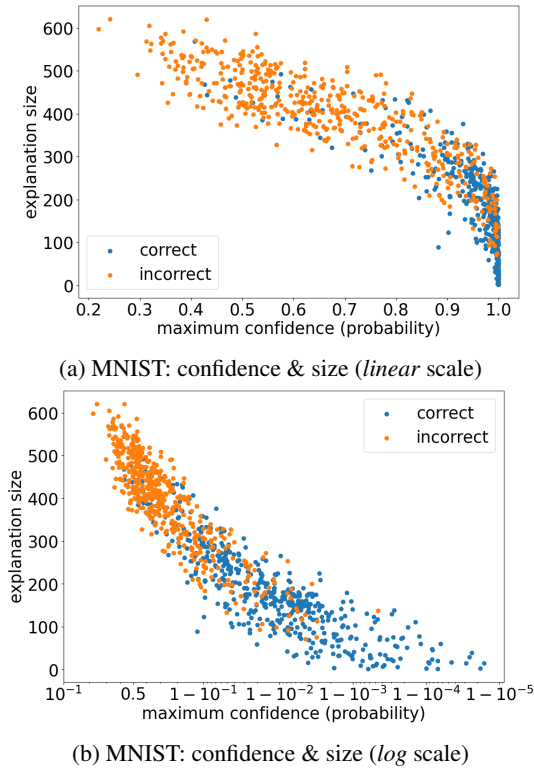


Figure 5: Maximum confidence and explanations size of *correctly* and *incorrectly* classified MNIST images in *linear* and *log* scales. As most probability values are in range $[0.9, 1]$, we also plot on *log scale* for better visualization.

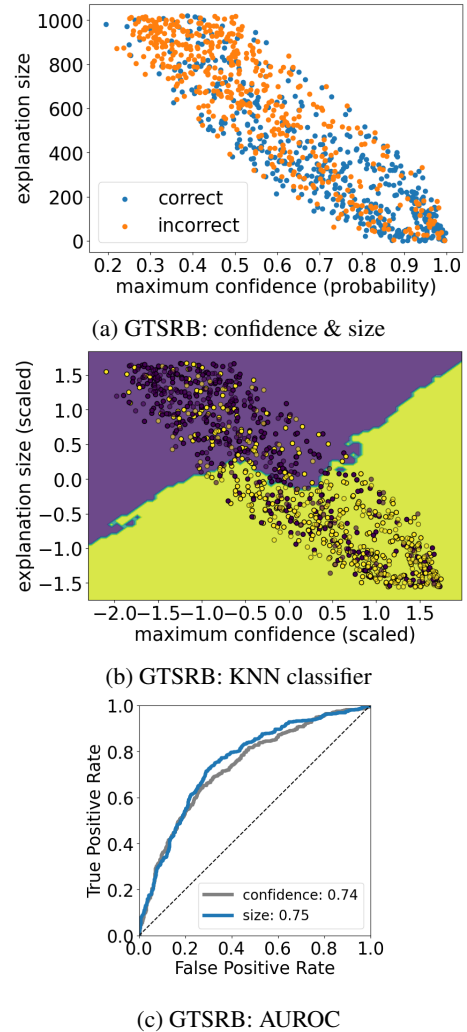
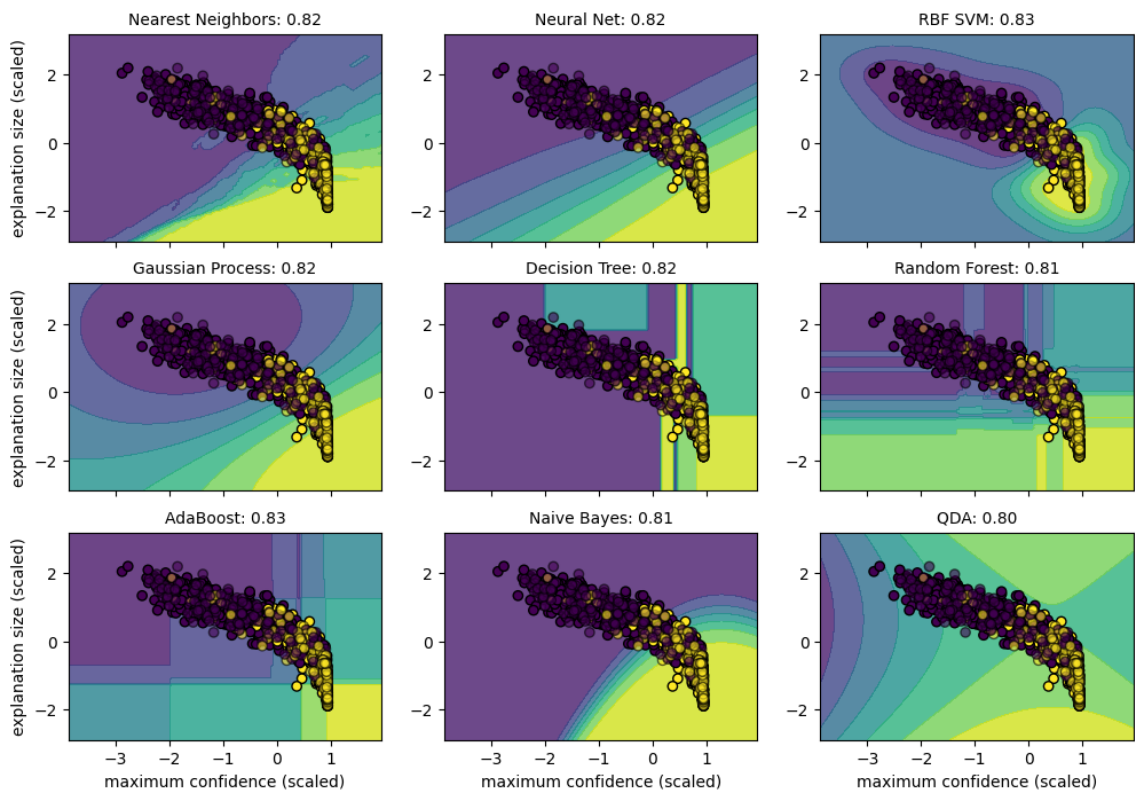
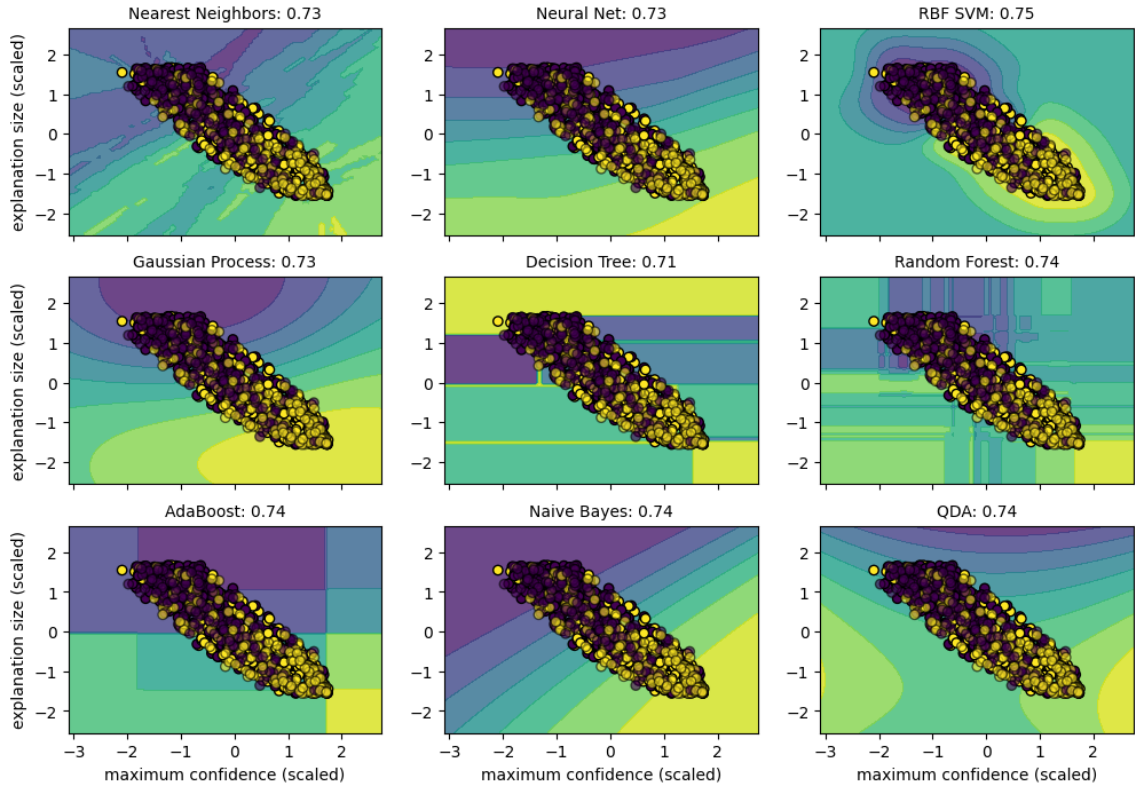


Figure 6: Detecting *incorrect* examples for GTSRB. (a) Correlation between maximum confidence and explanation size. (b) ROC curves and AUROC values. (c) A KNN classifier.



(a) MNIST



(b) GTSRB

Figure 7: Various classifiers using maximum confidence and explanation size to detect *correct* and *incorrect* examples in the MNIST (top) and GTSRB (bottom) datasets. Accuracy of each classifier is plotted above each sub-figure, e.g., Radial Basis Function Support Vector Machine (RBF SVM) achieves 83% and 75%, respectively.

B.2 Detecting out-of-distribution examples

Neural networks sometimes have high-confidence predictions when the test distribution is different from the training distribution, which poses a safety concern (Hein, Andriushchenko, and Bitterwolf 2019). We experimented using VERIX+ explanations as a method of detecting out-of-distribution samples. We trained models on the MNIST dataset and used GTSRB and CIFAR-10 images as out-of-distribution samples. We treated out-of-distribution as positive and evaluated the AUROC value using the softmax probability baseline as proposed by (Hendrycks and Gimpel 2017). In addition to results in Section 4.4, we also performed out-of-distribution detection on the fully-connected MNIST model. Results are presented in Figure 9. Our experiment results show that using explanation sizes as an indicator of out-of-distribution samples result in better AUROC values than the baseline for both types of models.

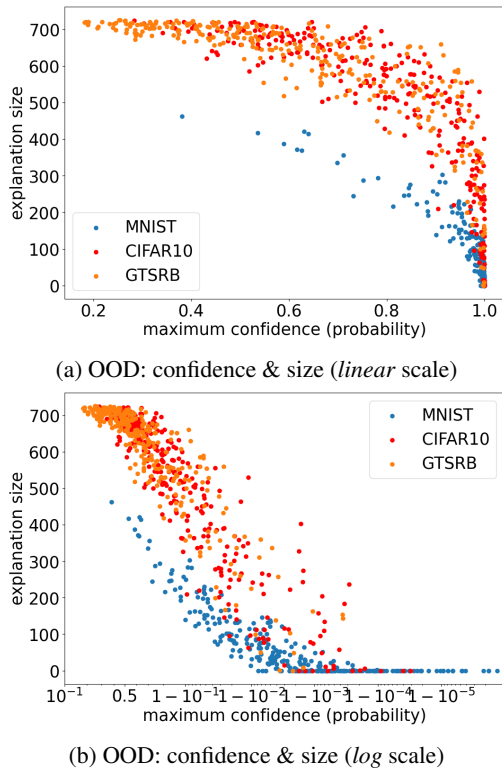


Figure 8: Maximum confidence and explanation size in *linear* and *log* scales of *in-distribution* (MNIST) and *out-of-distribution* (CIFAR10 and GTSRB) images that are classified by the MNIST-CNN model.

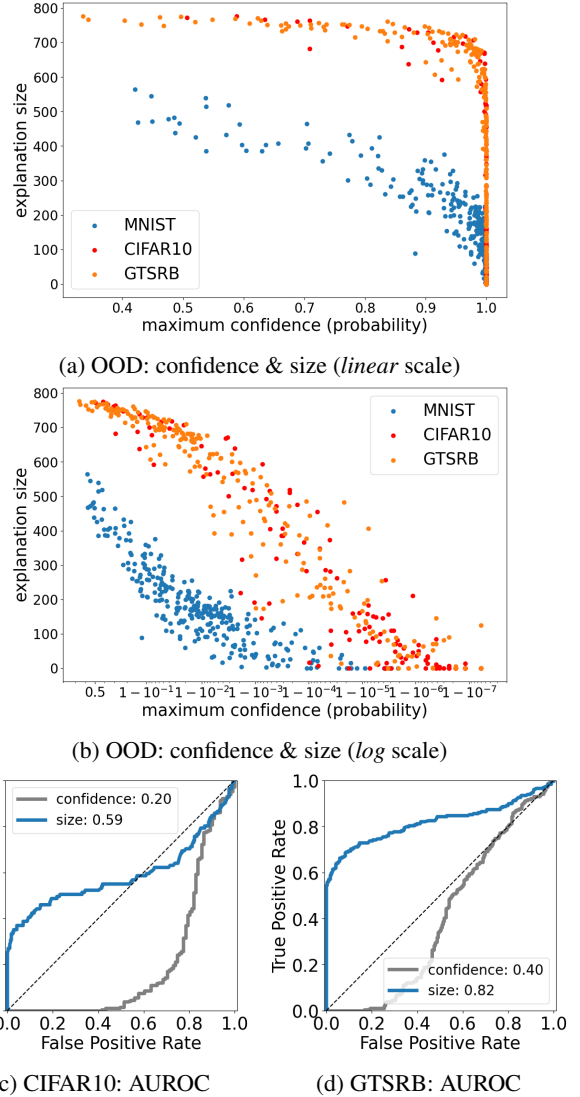


Figure 9: Detecting *out-of-distribution* examples from CIFAR10 and GTSRB for the MNIST-FC model. (a)(b) Maximum confidence and explanation size in *linear* and *log* scales. (c)(d) ROC curves and AUROC values for OOD samples from CIFAR10 and GTSRB, respectively.

C Model specifications

We evaluated our framework on standard image benchmarks including the MNIST (LeCun, Cortes, and Burges 2010), GTSRB (Stallkamp et al. 2012), and CIFAR10 (Krizhevsky et al. 2009) datasets, and trained both fully connected and convolutional models. Note that, when calling the Marabou (Katz et al. 2019; Wu et al. 2024) tool to perform the SOLVE functionality, in order for the queries to be *decidable*, the outputs of the networks need to be raw logits before the final softmax activation. For this, one needs to specify the `outputName` argument of the `read_onnx` function to be the pre-softmax logits. We remark that this does not change the decisions of a network. As a workaround for this, one can also train the model by setting `from_logits=True` in the loss function.

C.1 MNIST, GTSRB, and CIFAR10

The MNIST dataset is composed of gray-scale handwritten images of size $28 \times 28 \times 1$. The architectures of networks we trained on MNIST are shown in Table 3 for fully connected and Table 4 for convolutional. They achieve prediction accuracies of 93.76% and 96.29% respectively.

Table 3: Architecture of the MNIST-FC model.

Layer Type	Input Shape	Output Shape	Activation
Flatten	$28 \times 28 \times 1$	784	-
Fully Connected	784	10	ReLU
Fully Connected	10	10	ReLU
Output	10	10	-

Table 4: Architecture of the MNIST-CNN model.

Layer Type	Input Shape	Output Shape	Activation
Convolution 2D	$28 \times 28 \times 1$	$13 \times 13 \times 4$	-
Convolution 2D	$13 \times 13 \times 4$	$6 \times 6 \times 4$	-
Flatten	$6 \times 6 \times 4$	144	-
Fully Connected	144	20	ReLU
Output	20	10	-

The GTSRB dataset contains colored images of traffic signs with shape $32 \times 32 \times 3$. In order to obtain models with higher accuracies, we selected the 10 most frequent categories out of the 43 contained in the original dataset. The architecture of the fully connected model trained on GTSRB is in Table 5, and the convolutional model is shown in Table 6. The networks have 85.93% and 90.32% prediction accuracies, respectively.

Table 5: Architecture of the GTSRB-FC model.

Layer Type	Input Shape	Output Shape	Activation
Flatten	$32 \times 32 \times 3$	3072	-
Fully Connected	3072	10	ReLU
Fully Connected	10	10	ReLU
Output	10	10	-

Table 6: Architecture of the GTSRB-CNN model.

Layer Type	Input Shape	Output Shape	Activation
Convolution 2D	$32 \times 32 \times 3$	$15 \times 15 \times 4$	-
Convolution 2D	$15 \times 15 \times 4$	$7 \times 7 \times 4$	-
Flatten	$7 \times 7 \times 4$	196	-
Fully Connected	196	20	ReLU
Output	20	10	-

The CIFAR10 dataset also contains $32 \times 32 \times 3$ images from 10 different categories. The architectures of models used are shown in Tables 7 and 8.

Table 7: Architecture of the CIFAR10-FC model.

Layer Type	Input Shape	Output Shape	Activation
Flatten	$32 \times 32 \times 3$	3072	-
Fully Connected	3072	10	ReLU
Fully Connected	10	10	ReLU
Output	10	10	-

Table 8: Architecture of the CIFAR10-CNN model.

Layer Type	Input Shape	Output Shape	Activation
Convolution 2D	$32 \times 32 \times 3$	$15 \times 15 \times 4$	-
Convolution 2D	$15 \times 15 \times 4$	$7 \times 7 \times 4$	-
Flatten	$7 \times 7 \times 4$	196	-
Fully Connected	196	20	ReLU
Output	20	10	-

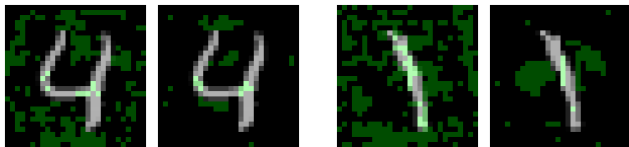
C.2 Adversarial training

Studies have shown that neural networks can be “fooled” by adversarial inputs crafted by applying a small perturbation to test samples so that they appear the same to human eyes but can cause neural networks to mis-classify them with high confidence. This can be mitigated by introducing adversarial samples when training the networks, known as *adversarial training* (Goodfellow, Shlens, and Szegedy 2014).

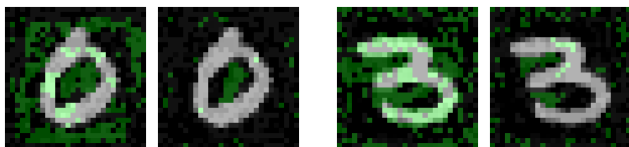
To adversarially train the MNIST-FC model, after each epoch of the training phase, we used projected gradient descent (PGD) attack to generate adversarial examples from 50% of randomly selected training samples, and then mixed them with the remaining training data. These malicious samples used for testing were crafted by applying PGD attack to a different MNIST network to avoid possible bias. MNIST-FC has a compromised accuracy of 23.66% on the malicious test set, while MNIST-FC-ADV achieves a much higher 82.66% due to adversarial training.

Table 9: Architecture of the MNIST model used to generate *malicious* samples in Section 4.2.

Layer Type	Input Shape	Output Shape	Activation
Flatten	$28 \times 28 \times 1$	784	-
Fully Connected	784	30	ReLU
Fully Connected	30	30	ReLU
Output	30	10	-



(a) MNIST-FC and MNIST-FC-ADV on *normal* inputs.



(b) MNIST-FC and MNIST-FC-ADV on *malicious* inputs.

Figure 10: Comparisons of explanations produced by normally trained MNIST-FC (left) and adversarially trained MNIST-FC-ADV (right) on both *original* (top) and *malicious* (bottom) inputs.

We investigated the differences in explanations sizes on adversarial inputs for both normally trained and adversarially trained networks. We separated correctly and incorrectly predicted inputs since adversarial samples result in more incorrect predictions, which correlates with bigger explanation sizes, as described in Section 4.3. We found that adversarial inputs often have larger explanation sizes, and adversarially trained networks tend to have smaller explanations.